



ANALYSIS OF THE FLOW AND THERMAL FIELDS IN BOBTAIL ROOFS HEATED FROM THE BASE WALL

Ola Kamiyo

okamiyo@unilag.edu.ng

University of Lagos, Lagos, Nigeria - Department of Mechanical Engineering

ABSTRACT

Analysis of airflow and thermal characteristics of attics of bobtail-shaped pitched roofs heated through a horizontally suspended ceiling is numerically carried out in this study. Pitch angles of 14° , 18° , 30° and 45° within the standard pitch roof range are selected. The configuration falls within Rayleigh number $3.19 \times 10^5 \leq Ra \leq 2.04 \times 10^7$. A finite-volume CFD code was used to solve the mass, momentum, and energy conservation equations governing the problem. The results obtained indicate a strong influence on the shape and angle of the roof. At lower roof pitches, the flow field is characterized by multiple counter-rotating vortices asymmetrically arranged within the enclosures. Eight cells in the 14° enclosure were reduced to five in the 45° roof pitch. The size and rotating strength of a vortex increase from the left corner to the middle of the enclosures. At higher pitch angles, the vertical wall obstructed the flow leading to a number of distorted cells. The maximum velocity within the aerodynamic boundary layer along the base wall occurs at $Y=0.02$ with the values $U=0.013$ and $U=0.028$ in the 14° and 45° enclosures respectively. The thermal field portrays a convection system of rising hot plumes from the base wall and descending cold jets from the inclined walls; all enclosed by thin boundary layers along the walls. Graphical plots of velocity and temperature variations along some cross-sections within the enclosures enable the prediction of some important heat and flow parameters.

Keywords: Airflow, thermal field, natural convection, attic, pitch roof, bobtail.

NOMENCLATURE

AR	Aspect ratio, $AR = 2H/L$
g	Acceleration due to gravity, m/s^2
H	Height of enclosure, m
L	Length of the enclosure, m
Pr	Prandtl number
Ra	Rayleigh number
T	Temperature, $^\circ K$
T_C	Temperature at the cold wall, $^\circ K$
T_H	Temperature at the hot wall, $^\circ K$
u	Velocity in the x-axis, m/s
U, V	Dimensionless velocity
v	Velocity in y-axis, m/s
X, Y	Dimensionless Cartesian coordinates

Greek symbols

α	Thermal diffusivity, m^2/s
β	coefficient of thermal expansion, $^\circ K$
θ	Dimensionless temperature
λ	Thermal conductivity, $W/m^\circ K$
ν	Kinematic viscosity, m^2/s
ρ	Density, kg/m^3
ϕ	Pitch angle, degrees

Received :17-11-2021

Accepted :26-1-2022

INTRODUCTION

Relevance of the airflow and heat transfer characteristics within enclosed surfaces to the designs of rooftops, ventilation and air-conditioning systems, solar equipment, and electronic boards cooling have made their areas of research focus over the years. Flack (1980) and Akinsete and Coleman (1982) introduced an investigation on the experimental and numerical modeling of pitched roofs. Thereafter, many studies on heat and fluid flow within the attic and across the ceiling have been carried out. Kamiyo et al. (2010) and Saha and Khan (2011) published exhaustive reviews on natural convection in triangular enclosures. In 2011, experimental and numerical investigation of natural convection and heat transfer in an inclined quadrantal cavity was reported by Yesiloz and Aydin (2011). They investigated the effects of the inclination angle and the Rayleigh number and found that the inclination angle significantly affects the heat transfer. Basak et al. (2013) used Bejan's headlines approach to study the natural convection in porous, right-angled triangular enclosures with a concave and a convex hypotenuse. Kamiyo et al. (2014) worked on the flow structure and temperature distribution in asymmetric triangular enclosures heated from below in which they analyzed the effects of the Rayleigh number and the pitch angle. Numerical investigation of natural convection in an isosceles triangular enclosure subjected to non-uniform cooling from the inclined surfaces and uniform heating from the base is reported by Saha and Gu (2015). Sieres et al. (2016) reported analytical and numerical computations of laminar natural convection in vertical upright-angled triangular cavities filled with air for selected pitch angles and a Rayleigh number range. Mirabedin (2016) formulated a correlation for Nusselt number in terms of its aspect ratio and Rayleigh number for heat transfer in a right-angled triangular enclosure and found that the Nusselt number increased with aspect ratio. Raj et al. (2018) performed combined natural convection and surface radiation experimental study on the influence of opening ratio (OR) on the temperature distribution within a vented triangular enclosure. In recent times, a number of complex roof shapes have been investigated. Cui *et al.* (2019) used a 3D numerical model approach to carry out transient free convection heat transfer in a triangular prismatic enclosure heated from the bottom wall and determined the critical Rayleigh number for the transition of the flow. Elnokaly et al. (2019) parametrically investigated the thermal performance of vaulted roofs with varying cross-section ratios and orientations in order to enhance the indoor thermal comfort of buildings in hot-arid regions. Mehryan et al. (2020) carried out a study on natural convection in a trapezoidal enclosure divided by a flexible partition. The results show that the heat transfer rate in the 30° trapezoidal cavity was found to be 15% lower than that in a square cavity. Kamiyo (2020) performed a numerical simulation of natural convective flow within a raised-ceiling rooftop when heated from below. Besides, a number of other complex roof shapes have also been investigated. However, there are many common ones that have not been studied sufficiently. The bobtail roof considered in this study is one. This study, therefore, adopts a finite-volume CFD package to investigate the airflow and temperature distribution within the attic of a bobtail roof, shown in Figure(1), when heated through the base wall. The investigated parameters fall within the aspect ratio (AR) range $0.25 \leq AR \leq 1.00$ and Rayleigh number $3.19 \times 10^5 \leq Ra \leq 2.04 \times 10^7$.

METHODOLOGY

The attic space considered is within a long, horizontal bobtail roof which extends more than double its width in the direction perpendicular to its cross-section as shown in Figure(1). According to Penot and N'Dame (1992), the flow and thermal fields within such geometric structure could be regarded as two-dimensional. The bobtail shape is simply an isosceles triangle truncated on one of the inclined sides. The shape used in this study is truncated on the right side at the three-quarter of the base length.

The roof in Figure(1) consists of a horizontal ceiling assumed to be made of gypsum, two inclined walls made of aluminum sheets, and a vertical concrete wall. The roof and ceiling trusses are neglected. The air-filled attic has no internal heat generation. The computational domain dimensions alongside the boundary conditions are normalized due to the variation in the sizes of roofs generally. The equations governing the laminar flow problem at a steady state when subjected to the Boussinesq approximation (Gray and Giorgini (1976); Ridouane *et al.*, (2005)), are expressed in dimensionless forms as:

Conservation of Mass:

$$\frac{\partial U}{\partial X} + \frac{\partial V}{\partial Y} = 0 \tag{1}$$

Conservation of Momentum:

X-momentum:

$$U \frac{\partial U}{\partial X} + V \frac{\partial U}{\partial Y} = -\frac{\partial P}{\partial X} + Pr \left(\frac{\partial^2 U}{\partial X^2} + \frac{\partial^2 U}{\partial Y^2} \right) \tag{2}$$

Y-momentum:

$$U \frac{\partial V}{\partial X} + V \frac{\partial V}{\partial Y} = -\frac{\partial P}{\partial Y} + Pr \left(\frac{\partial^2 V}{\partial X^2} + \frac{\partial^2 V}{\partial Y^2} \right) + RaPr\theta \tag{3}$$

Conservation of Energy:

$$U \frac{\partial \theta}{\partial X} + V \frac{\partial \theta}{\partial Y} = \left(\frac{\partial^2 \theta}{\partial X^2} + \frac{\partial^2 \theta}{\partial Y^2} \right) \tag{4}$$

where $X, Y = \frac{y}{L}, V = \frac{vL}{\alpha}, U = \frac{uL}{\alpha}, P = \frac{pL^2}{\rho\alpha^2}, Pr = \frac{\nu}{\alpha},$ and $Ra = \frac{g\beta(T_H - T_C)H^3}{\alpha\nu}.$

Boundary conditions:

Velocity:

$$U = V = 0 \quad (\text{no slip condition along the walls})$$

Temperature:

$$\theta = 1 \quad (\text{isothermal hot ceiling})$$

$$\theta = 0 \quad (\text{isothermal cold inclined walls})$$

$$d\theta = 0 \quad (\text{adiabatic vertical wall})$$

Four pitch angles that are commonly used within the standard roof range are selected. The parametric details of the enclosures are given in Table 1. Very Fine unstructured triangular mesh was generated for the computational domain. The grid for the 14° roof pitch is as shown in Figure(2). The coupled, partial differential conservation equations (1) – (4) were solved numerically using a finite-volume-based ANSYS FLUENT® (V-18) solver. The pressure-velocity coupling was tackled using the SIMPLE algorithm. Pressure interpolation was addressed using the PRESTO scheme. A QUICK scheme was used to spatially discretize the momentum and energy equations. To ensure proper convergence, the convergence target for the continuity equation was fixed at 10⁻⁵ while that for the momentum and energy equations was put at 10⁻⁷. The governing equations were solved iteratively to obtain a converged solution for each roof pitch enclosure. To test the grid independence of the results, some

numerical runs were performed for different numbers of elements. The results for the mean Nusselt number obtained for each grid is shown in Table 2 for the 14° roof pitch. The tests continued until a grid change of 16% in the number of elements produced a result change of less than 1%. It is then concluded that a mesh of about 65,000 elements is good enough to produce grid-independent results for the roof pitch. The capability of the ANSYS FLUENT CFD package used in this study to effectively carry out the numerical computation of the laminar natural convection in the attics of bobtail roofs heated from the base wall investigated is premised on the work of Yesiloz and Aydin (2013). In it, they compared the results of the numerical analysis of laminar natural convection in a right-angled triangular enclosure heated from below carried out using ANSYS FLUENT with the results of an experiment with the same configuration and Rayleigh number range of 10^3 to 10^7 . The results are found to be in good agreement. It is then resolved that ANSYS FLUENT code would effectively simulate the problem.

RESULTS AND DISCUSSION

The results obtained for the flow field are presented in the form of streamlines, air velocity contour plots and graphical plots of air velocity variations across vertical lines at $X = 0.25, 0.5, 0.66,$ and 0.8 and horizontal lines at heights $Y = 0.05$ and 0.2 in Figures(3-6). The thermal field results are shown in Figures(7-9) as temperature contour plots and temperature variations along the same cross-sectional lines.

Streamlines

The streamlines for the enclosures are as shown in Figure(3). As the base wall gets heated, streams of hot air driven upward by buoyancy hit the cold inclined walls and split. In the process, a major part of the heat content is lost. Detaching from the upper wall under gravity, dense cold jets of air flow down to the base wall. This is reheated to repeat the process. At steady-state, this convection process results in a system of multiple counter-rotating vortices similar to the classical Rayleigh-Bernard convection. Holtzman et al. (2000) obtained a similar flow pattern as in this study with multiple cells in the experiments conducted in an isosceles triangular enclosure heated from the base wall. Figure(3-a) for the 14° roof pitch shows eight asymmetrically-arranged recirculating cells with the truncated side having only one large cell. The size and strength of the vortices increase from the left corner to the midsection. In the 18° enclosure, the number of cells has reduced to six. The two large counter-rotating vortices at the midsection of the enclosure in Figure(3-a) have merged to form the main vortex rotating anticlockwise. The sizes of other secondary cells only marginally increase. When the roof pitch is low, the effect of the vertical wall on the shape of the cell adjacent to it appears unnoticeable. In the 30° enclosure, however, the large cell, rotating clockwise, becomes distorted on hitting the wall. The deflected cell revolving with high strength equally distorted the main vortex at the midsection. The relatively chaotic situation near the vertical wall results in flow separation that led to the formation of a small cell rotating anticlockwise at the lower right corner. In the 45° roof pitch, the number of vortices reduced to five; two large counter-rotating distorted vortices at the middle and three small vortices near the bottom corners.

Velocity Distribution

Air velocity distribution in each of the roof enclosures is shown in Figure(4). In all the enclosures, air movement is relatively high along with the plumes and the jets located between adjacent cells. Air velocity is found to reduce from the outer circumference of a vortex to its core. As the roof pitch increases, the average velocity across the attic reduces

In Figure(5), the variations of the air velocity along the vertical lines at $X = 0.25, 0.66,$ and 0.8 for each of the roof pitch enclosures are presented. The line at $X = 0.25$ shows the flow situation near the intersection of the hot and cold walls. The line at $X = 0.66$ coincides with the upper vertex thereby analyzing the flow at the midsection. The line at $X = 0.8$ reveals the flow condition near the vertical wall. In the 14° enclosure, at $X = 0.25$, the line goes across the third cell from the left corner and the aerodynamic boundary layers at the lower and upper walls. Hence, velocity increases away from the base wall to the location of the maximum velocity within the boundary layer, then reduces from the lower part of the outer circumference of the cell to its core. It then increases towards the upper side of the circumference before decreasing in the upper boundary layer. In the 18° and 30° enclosures, the vertical line also crosses a cell. But in the 45° enclosure, it goes across the second and third cells. For the vertical line that goes to the upper vertex at $X = 0.66$, in the 14° enclosure, it follows the path of a decelerating plume. In the 18° enclosure, it crosses the main vortex at the midsection. The line shows the velocity variation across the distorted cells in the 30° enclosure. The wiggle in the 45° enclosure shows the velocity fluctuation that depicts the chaotic flow at the midsection. In all the enclosures, the velocity profile shows clearly the location of the maximum velocity (U_{max}) within the aerodynamic boundary layer along the walls. At the midsection ($X = 0.66$), the boundary layer thickness, $Y=0.02$, is surprisingly the same for all enclosures. In the 14° enclosure, U_{max} at 0.0131 doubles that in the 18° roof pitch while its value in the 45° roof pitch, 0.0288 , is twice that in the 14° enclosure. At $X = 0.8$ near the vertical wall, the vertical line in the 14° enclosure crosses the right edge of the largest or the seventh cell. The line passes through the left edge of the cell beside the vertical wall in the 18° enclosure. In the 30° and 45° enclosures, the vertical line passes through the distorted main vortex. Generally, the plots shown in Figure(5) enable the prediction of the width of a vortex, the strength of a plume or jet at a location, the thickness of the aerodynamic boundary layer along a wall, and the values of the air velocity along a vertical cross-section within the attic of a roof when within the pitch angles considered in this study. Velocity distributions along horizontal lines at heights $Y = 0.05$ and $Y = 0.2$ for the enclosures are shown in Figure(6). At height $Y = 0.05$, within the aerodynamic boundary layer along the base wall, the plots indicate velocity fluctuations that are due to the impact of the impinging jets. However, as the pitch angle increases, the flow becomes smooth. For the line at $Y = 0.2$, the velocity profile follows the parts of the cells that fall on the line. The crests correspond to the paths of the plumes and jets while the troughs fall within the cores of the cells. In the 30° and 45° enclosures, there are wiggles on the right half of the plots which is due to the deflection of the nearby cell by the vertical wall.

Temperature Field

Figure(7) shows the contour plots of the temperature distribution within the enclosures. The thermal field characteristically shows hot air rising from the hot base wall, in form of plumes, interposed with jets of cold air flowing down from the inclined walls. Thin thermal boundary layers are also formed along the walls. The half of a plume and half of an adjacent jet combined to form a cell. Therefore, a plume or a jet falls between adjacent counter-rotating cells. In the 14° enclosure, the thorough mixing of air by the multiple vortices results in uniform temperature across the enclosure. As the roof pitch increases, the volume of air to be heated within the attic increases. Consequently, with a constant hot-wall length, the heating effect reduces and hence the average temperature in the enclosure reduces; tending towards that of the cold wall. Haese and Teubner (2002) obtained a similar result for their work on heat transfer within an attic space. The temperature profiles along vertical lines at $X = 0.25, 0.5, 0.66,$ and 0.8 are presented in Figure(8) to show the effect of heating by the base wall across the enclosures. For the vertical line at $X = 0.25$ in the 14° enclosure, near the bottom

left corner, the line passed through the thermal boundary layer on the base wall, then part of a jet and part of a plume before the thermal boundary layer at the upper wall. The same pattern is observed in the 30° enclosure. In the 18° and 45° roof enclosures, the vertical line follows the path of a descending jet. The thermal boundary layer is well pronounced along the base wall and the inclined wall. At $X = 0.5$, the vertical line passes through the path of a rising plume in the 14° enclosure. In the other enclosures, after going through the thermal boundary layer, the line crosses part of a jet and then part of a plume before passing through the upper boundary layer. In the thermal boundary layer on the base wall of the 18° roof pitch, the air temperature has a maximum value of 0.43 at location $Y = 0.14$ within the boundary layer. Almost the same values are observed in the 30° enclosure. For the vertical line at $X = 0.66$ which goes to the upper vertex, in the 14° enclosure, the line follows the path of a descending jet. It goes mainly along a plume in the 30° enclosure. The line crosses part of a jet and part of a plume in the 18° and 45° enclosures. At $X = 0.8$ near the vertical adiabatic wall, the vertical line tracks the path of a plume in the 14° and 18° enclosures. It shows the temperature values across a distorted jet in the 30° and 45° enclosures. The temperature profiles at vertical cross-sections within the enclosures, as shown in Figure(8), could be used to predict the thermal condition at any point within the attic of the same configuration. Figure(9) shows air temperature variation along horizontal lines at heights $Y = 0.05$ and $Y = 0.2$ in each enclosure. The horizontal line at $Y = 0.05$ falls within the thermal boundary layer on the base wall in all the enclosures. The plot indicates the temperature values at the base of the rising plumes and as the cold jets fall on the base wall. At height $Y = 0.2$, the horizontal line cut across the major part of the interior of the enclosures. The crests signify the temperature value when the line crosses the middle of hot plumes while the troughs indicate temperature value at the middle of cold jets. The temperature variation pattern is synchronous with the flow field within each enclosure. The number of crests reduces as the pitch angle increases. The width between a crest and an adjacent trough gives the length of a chord of a cell. The practical benefits of the results obtained in this study include their applications in rooftop storage of sensitive materials that are susceptible to temperature and moisture variations.

CONCLUSIONS

Analysis of the airflow and thermal fields in the attic of a bobtail-shaped pitched roof heated from the base wall has been numerically investigated under steady-state conditions. Due to the asymmetric nature of the roof structure, the full enclosure has been studied with two-dimensional approximations. Roof pitch angles of 14°, 18°, 30° and 45° within the standard pitch roof range are selected. The geometric and thermal boundary conditions result in Rayleigh numbers ranging between 10^5 and 10^7 . At lower roof pitch, the flow field is characterized by multiple counter-rotating vortices asymmetrically arranged within the enclosures. The number of cells formed decreases as the roof pitch increases. Eight cells in the 14° enclosure were reduced to five in the 45° roof pitch. The size and rotating strength of a vortex increase from the left corner to the middle of the enclosures. At higher pitch angles, the vertical wall obstructed the flow leading to a number of distorted cells. The thermal field portrays a convection system of rising hot plumes from base wall and descending cold jets from the inclined walls; all enclosed by thin boundary layers along the walls. Graphical plots of velocity and temperature variations along some cross-sections within the enclosures enable the prediction of the diameter of a vortex, the strength of a plume or jet at a location, the thickness of boundary layers, and the values of velocity and temperature at a location within an attic with the pitch angles considered. This knowledge is useful to rooftop designers and building users.

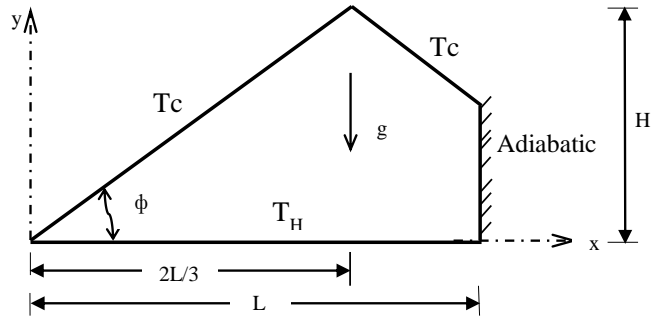


Fig. 1. Physical model

Table 1. Parametric details of the enclosures

Pitch Angle (ϕ)	14°	18°	30°	45°
Aspect Ratio (AR)	0.25	0.325	0.58	1.00
Rayleigh Number (Ra)	3.19×10^5	7.00×10^5	3.98×10^6	2.04×10^7

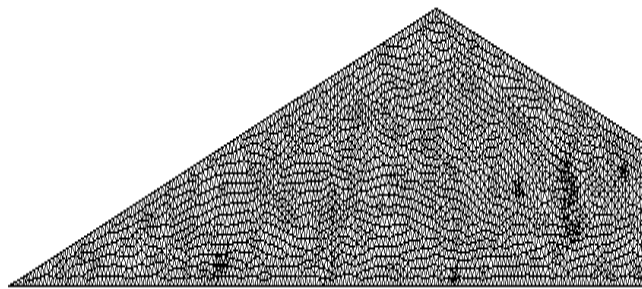
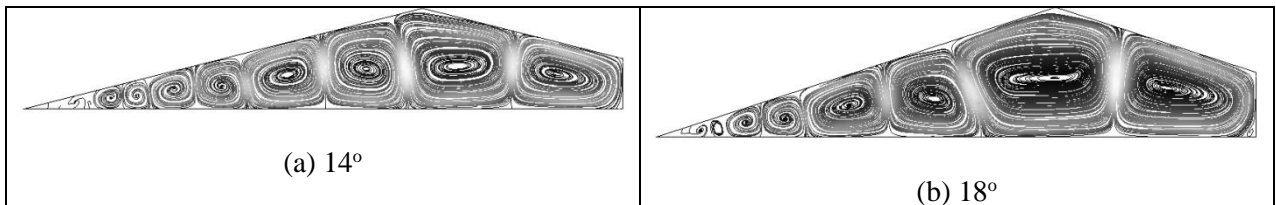


Fig. 2. Computational grid for the 14° pitch enclosure

Table 2. Grid independence test for the 14° roof pitch enclosure

Number of elements	43,919	55,897	65,143	75,634
Nu	15.662	20.958	21.596	21.645



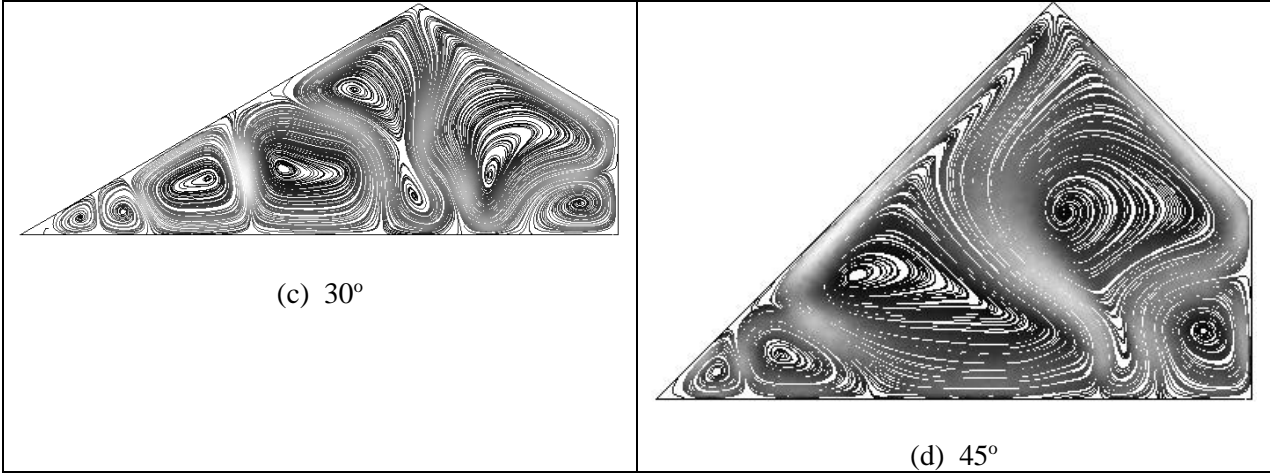


Fig. 3. Streamlines for different roof pitch enclosures

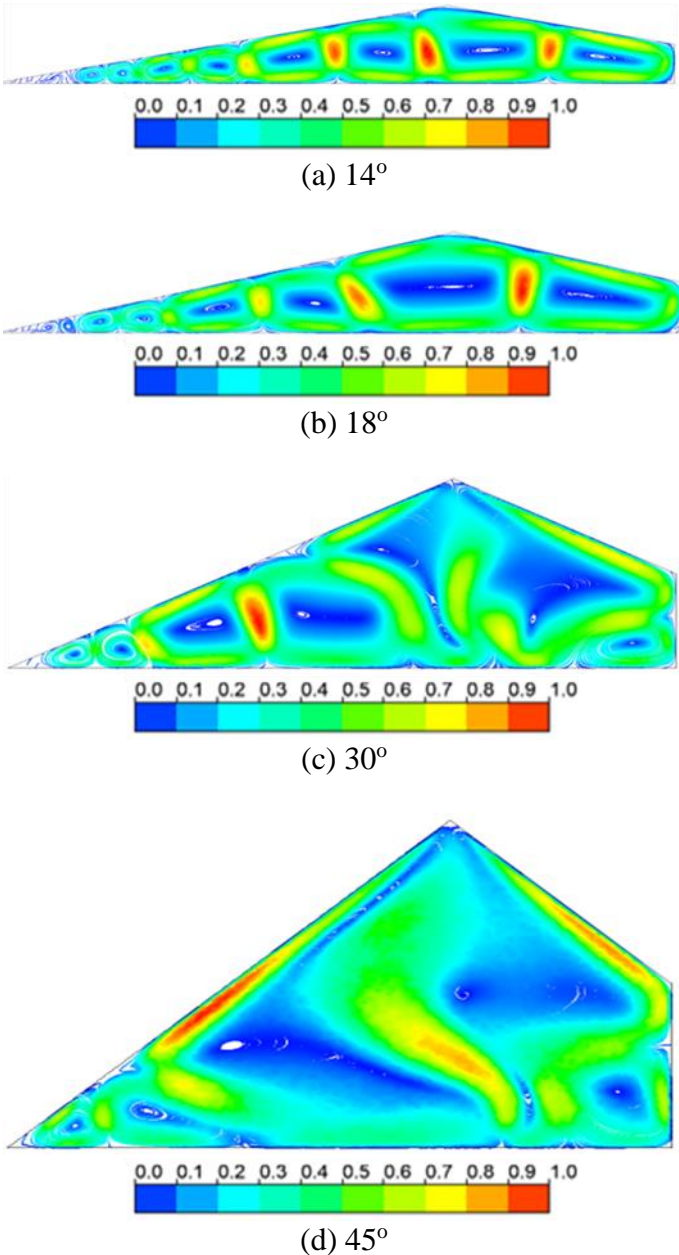


Fig. 4. Air velocity distribution for different roof enclosures

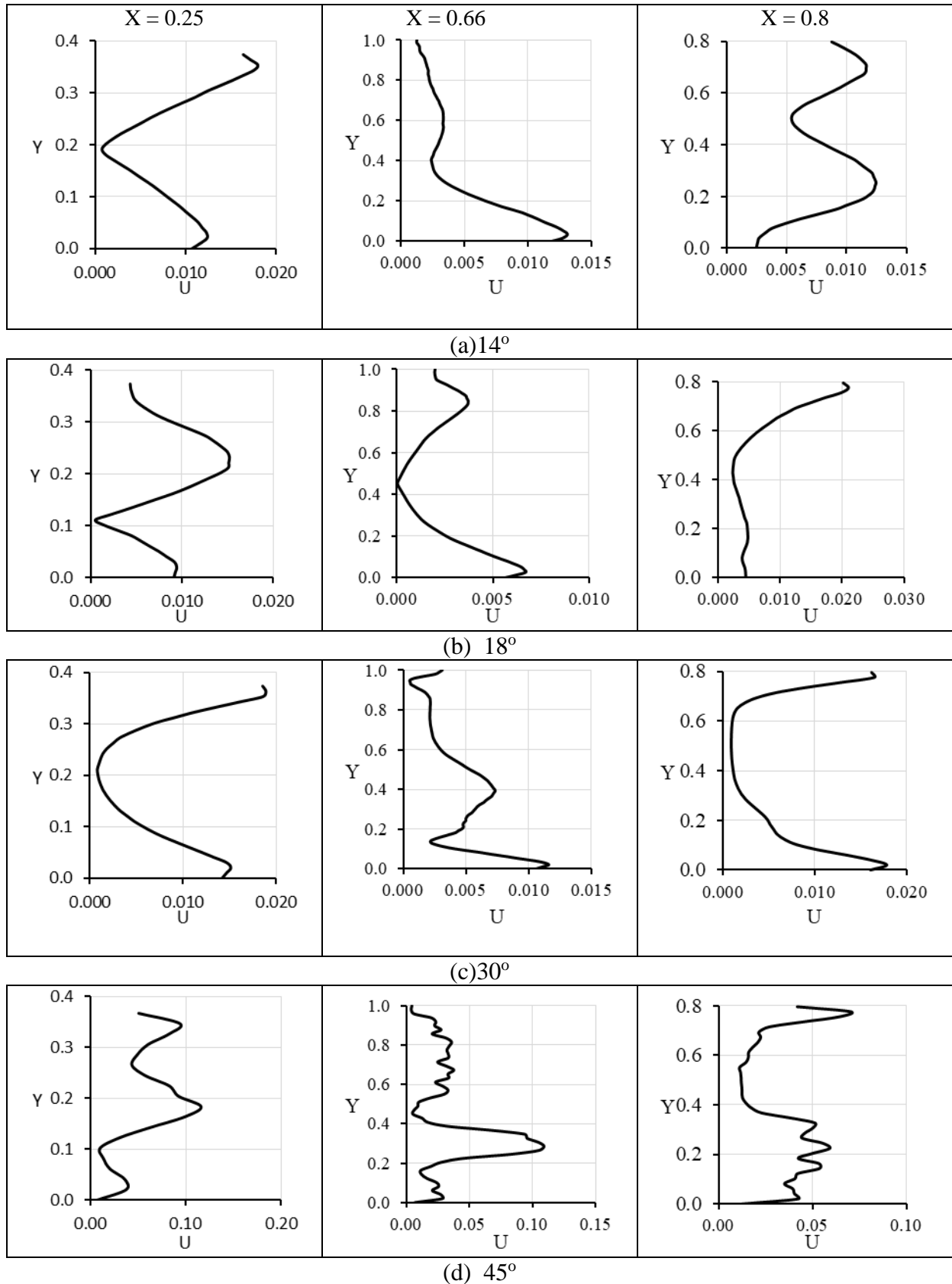


Fig. 5. Air velocity variations along vertical lines at selected points along X in each enclosure

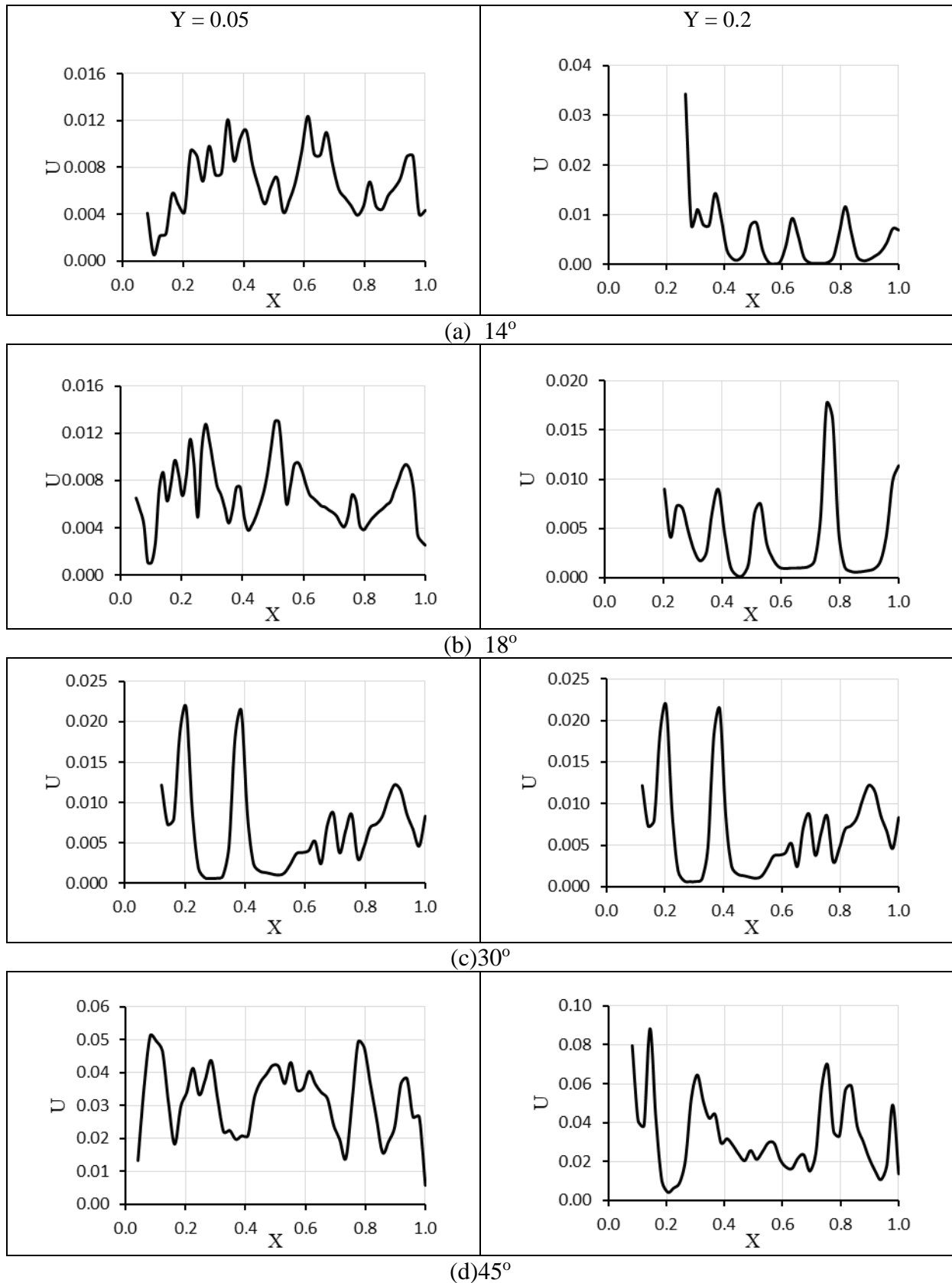


Fig. 6. Velocity variation along horizontal lines at height $Y = 0.05$ and $Y = 0.2$ for different roof pitch enclosures

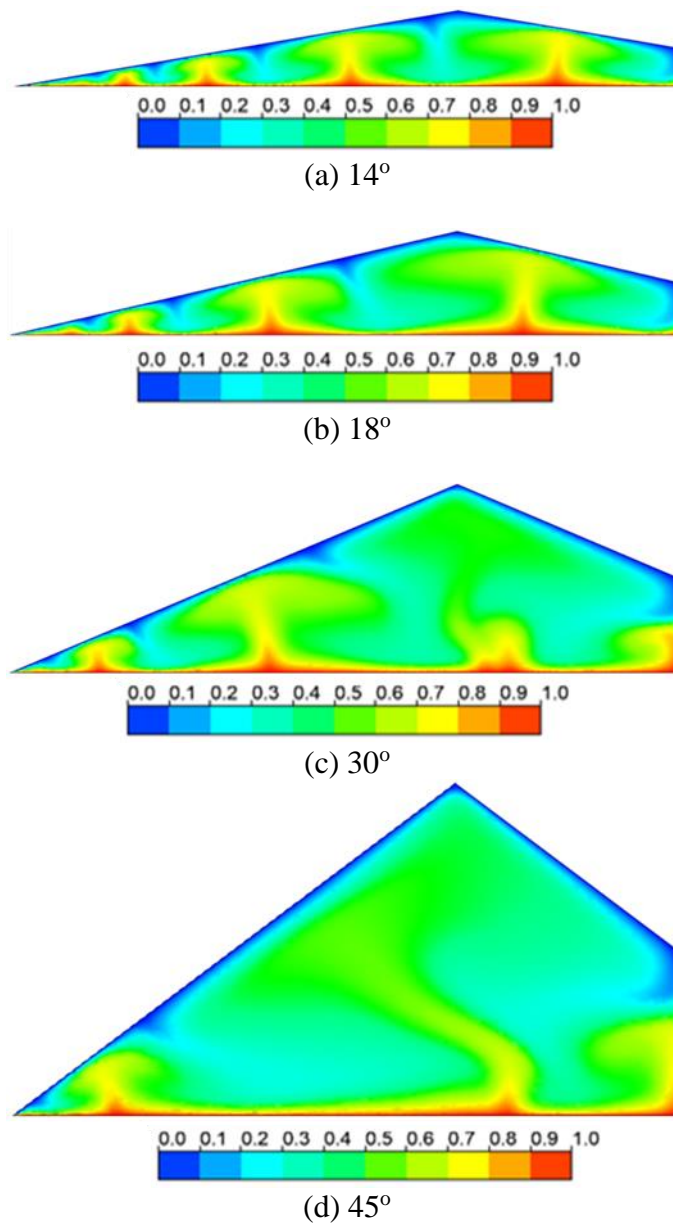
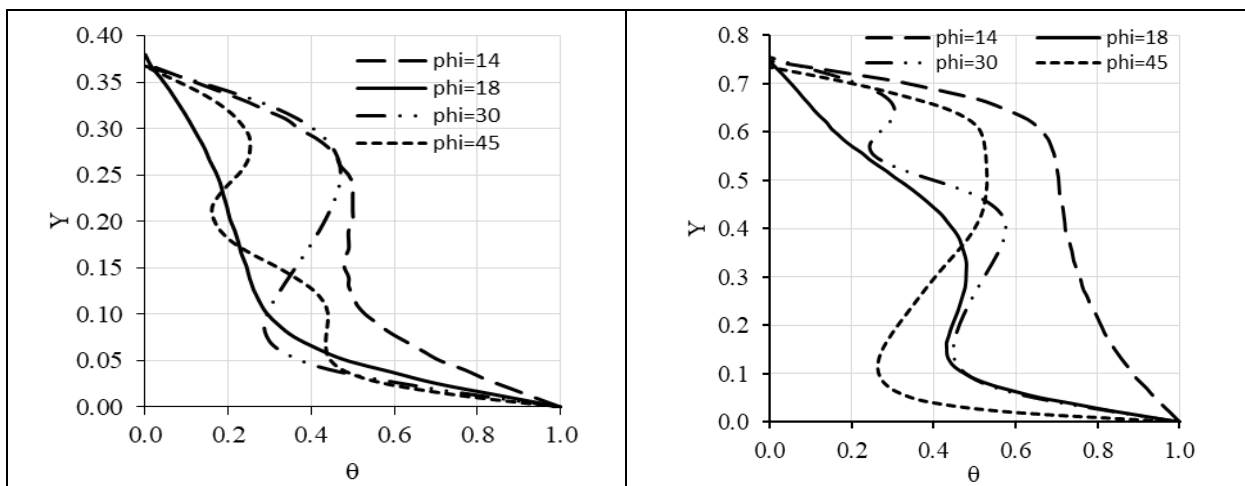


Fig.7. Temperature distributions for different roof enclosures



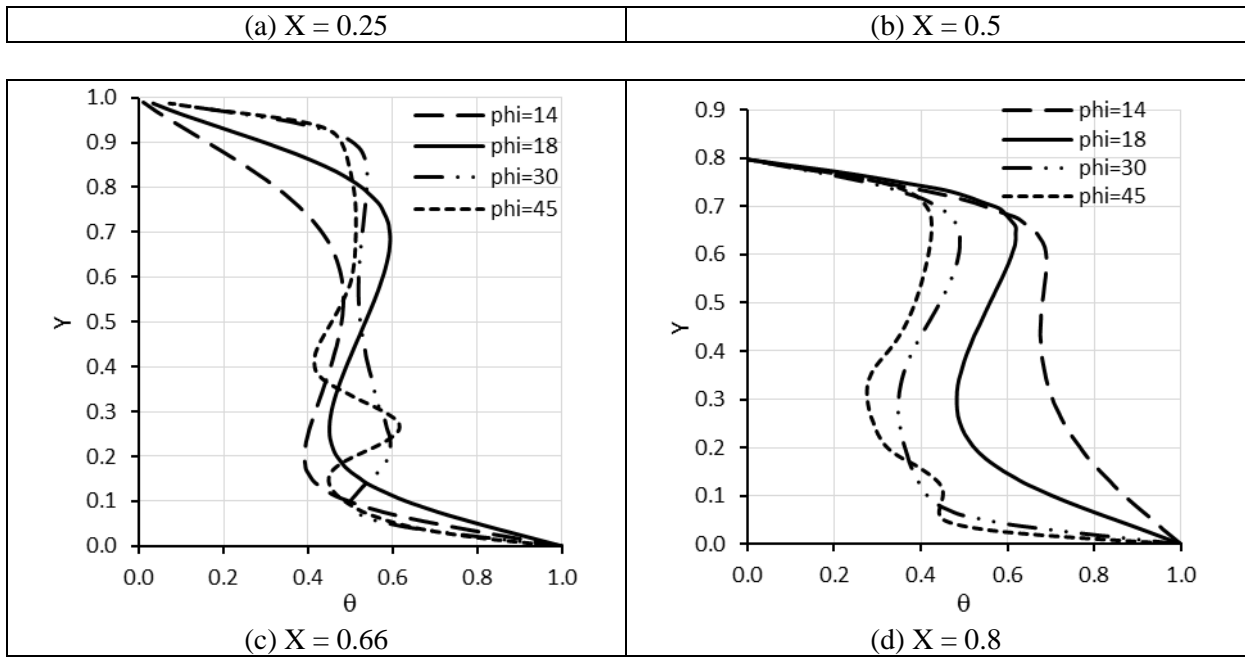
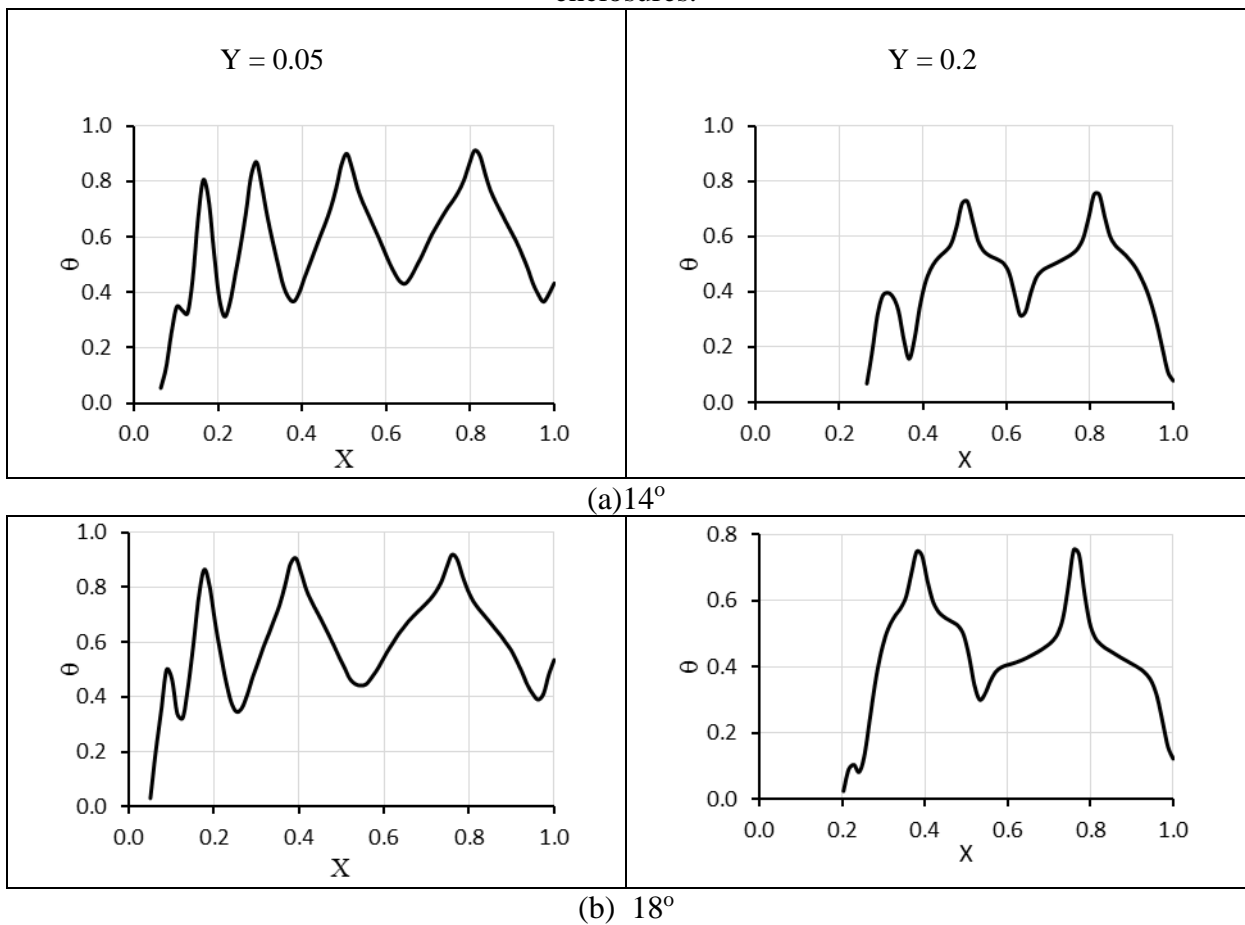


Fig. 8. Temperature profiles along vertical lines at selected points along X in the roof enclosures.



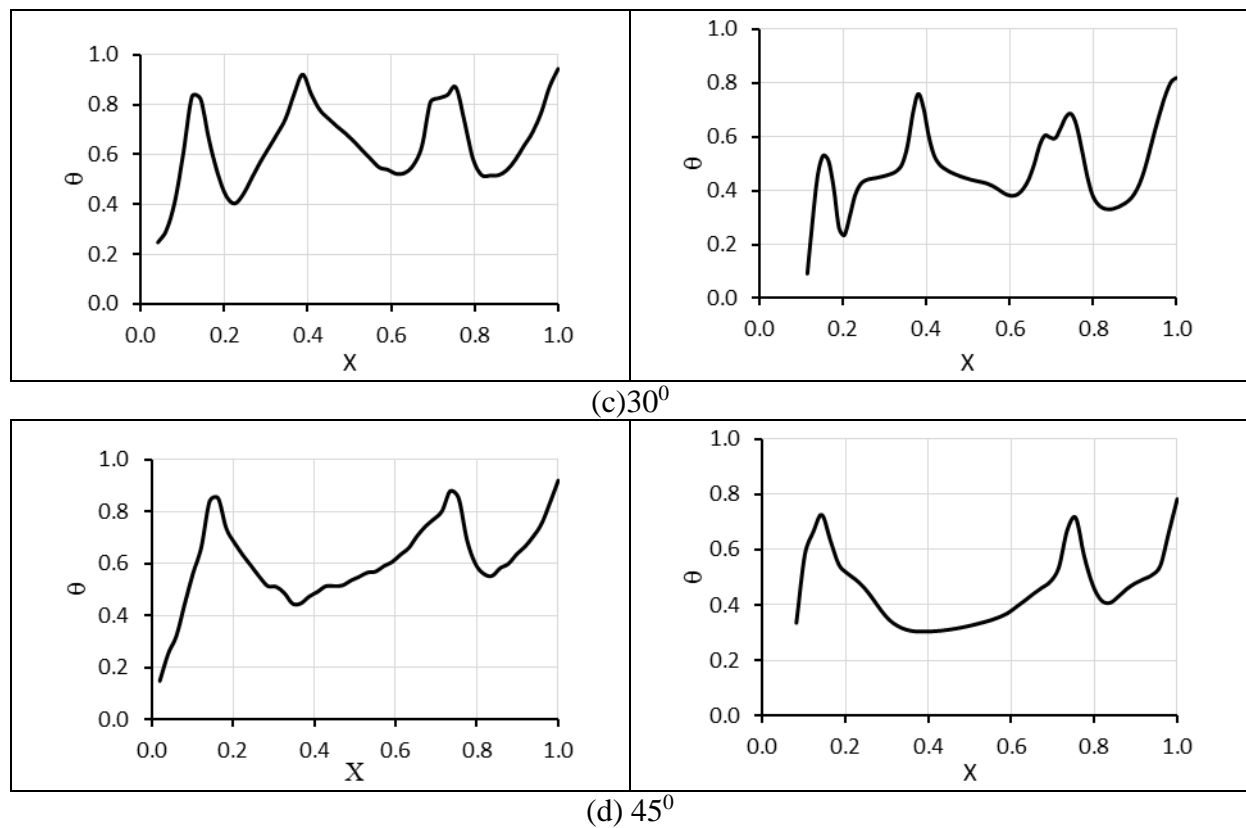


Fig. 9. Air temperature across heights $Y = 0.05$ and $Y = 0.2$ for different enclosures

REFERENCES

Akinsete, V.A. , Coleman T.A., Heat transfer by steady laminar free convection in triangular enclosures, *IJHMT*, Vol.25, No.7, pp.991-998, 1982. [doi.org/10.1016/0017-9310\(82\)90074-6](https://doi.org/10.1016/0017-9310(82)90074-6)

Basak, T., Anandalakshmi, R. and Biswal, P., Analysis of convective heat flow visualization within porous right-angled triangular enclosures with a concave/convex hypotenuse, *Num. Heat Transfer, Part A: Applications*, Vol.64, No.8, pp.621-647, 2013. doi.org/10.1080/10407782.2013.790265

Cui, H., Xu, F., Sahad, S. and Liu, Q., Transient free convection heat transfer in a section triangular prismatic enclosure with different aspect ratios, *Int. J. Thermal Sciences*, Vol.139, pp.282-291, 2019. doi.org/10.1016/j.ijthermalsci.2019.02.023

Elnokaly, A., Ayoub, M. and Elseragy, A., Parametric investigation of traditional vaulted roofs in hot-arid climates', *Renewable Energy*, Vol.138, pp.250-262, 2019. doi.org/10.1016/j.renene.2019.01.061

Flack, R. D., The experimental measurement of natural convection heat transfer in triangular enclosures heated or cooled from below, *J. Heat Transfer*, Vol.102, pp.770-772, 1980. doi.org/10.1115/1.3244389

Gray, D.D. and Giorgini, A., The validity of the Boussinesq approximation for liquids and gases, *IJHMT*, Vol.19, pp.545-551, 1976. [doi.org/10.1016/0017-9310\(76\)90168-X](https://doi.org/10.1016/0017-9310(76)90168-X)

Haese, P.M. and Teubner, M. D., Heat exchange in an attic space, *IJHMT*, Vol.45, pp.4925-4936, 2002. [doi.org/10.1016/S0017-9310\(02\)00208-9](https://doi.org/10.1016/S0017-9310(02)00208-9)

Holtzman, G.A., Hill, R.W. and Ball, K.S., Laminar natural convection in isosceles triangular enclosures heated from below and symmetrically cooled from above, *JHT*, Vol.122, No.3, pp.485-491, 2000. doi.org/10.1115/1.1288707

Kamiyo, O., Numerical simulations of natural convection for raised-ceiling rooftop heated from below, *KJE*, Vol.11, No.4, pp.58-71, 2020. dx.doi.org/10.30572/2018/kje/110405

Kamiyo, O.M., Angeli, D., Barozzi, G.S. and Collins, M.W. Natural convection in asymmetric triangular enclosures heated from below, *J. Phys.: Conf. Ser.* 547, 012043, 2014.

Kamiyo, O. M., Angeli, D., Barozzi, G.S., Collins, M.W., Olunloyo, V.O.S. and Talabi, S.O., A comprehensive review of natural convection in triangular enclosures, *AMR Trans. ASME*, Vol.63, No.6, pp.1-13, 2010. doi.org/10.1115/1.4004290

Mehryan, S.M., Mohammad, G., Reza, K.F., Ahmad, H. and Mohsen, I., Free convection in a trapezoidal enclosure divided by a flexible partition, *IJHMT*, Vol.149, pp.1-14, 119186, 2020. doi.org/10.1016/j.ijheatmasstransfer.2019.119186

Mirabedin, S., CFD modelling of natural convection in right-angled triangular enclosures', *Inter. J. Heat Technology*, Vol.34, No.3, pp.503-506, 2016. doi: 10.18280/ijht.340322

Penot, F. and N'Dame, A., Successive bifurcations of natural convection in a vertical enclosure heated from the side, *Heat Transfer: 3rd UK National Conference and First European Conference on Thermal Sciences*, UK, Vol.1, pp.507-513, 1992.

Raj, R., Pradyumna, K. C., Rakshith, B.R., Nithin, R.B. and Karthik, S.R., Combined natural convection and surface radiation inside vented triangular enclosure- an experimental study, *International Conference on Research in Mechanical Engineering Sciences*, Vol.144, 04019, 2018. doi.org/10.1051/mateconf/201814404019

Ridouane, E. H., Campo, A. and McGarry, M., Numerical computation of buoyant airflows confined to attic spaces under opposing hot and cold wall conditions, *Inter. J. Thermal Sciences*. Vol.44, No.10, pp.944–952, 2005. doi.org/10.1016/j.ijthermalsci.2005.03.008

Saha, S.C. and Gu, Y.T., Natural convection in a triangular enclosure heated from below and non-uniformly cooled from top, *IJHMT*, Vol.80, pp.529–538, 2015. doi.org/10.1016/j.ijheatmasstransfer.2014.09.047

Saha, S.C. and Khan, M.M.K., A review of natural convection and heat transfer in attic-shaped space, *Energy and Building*, Vol. 43, pp.2564-2571, 2011. doi.org/10.1016/j.enbuild.2011.06.020

Sieres, J., Campo A. and Martinez-Suarez, J.A., Natural convection airflow in vertical upright –angled triangular cavities under realistic thermal boundary conditions, *Thermal Science*, Vol.20, No.5, pp.1407-1420, 2016. doi.org/10.2298/TSCI130530018S

Yesiloz, G. and Aydin, O., Natural convection in an inclined quadrantal cavity heated and cooled on adjacent walls, Experimental Thermal and Fluid Science, Vol.35, pp.1169–1176, 2011. doi.org/10.1016/j.expthermflusci.2011.04.002